Physicochemical characterization of natural sand from the south-east of Morocco and its potential use as sorbent for dyes removal

A. Elhalil[a], M. Barour[a], H. Tounsadi[a,b,*], R. Elmoubarki[a], E.M. Lemdek[a], M. Sadiq[a], M. Abdennouri[a], F.Z. Mahjoubi[c], S. Qourzal[d], N. Barka[a]

[a]Laboratoire LS3M, Université Sultan Moulay Slimane, FP Khouribga, B.P. 145, 25000 Khouribga, Morocco, Tel. +212 645208564;
Fax: +212 523 49 03 54; emails: hananetounsadi@gmail.com (H. Tounsadi), elhalil.alaaeddine@gmail.com (A. Elhalil),
barourmohammed1@gmail.com (M. Barour), elmoubarkirachid@gmail.com (R. Elmoubarki), lemdek@yahoo.fr (E.M. Lemdeg),
sadiqmhamed@hotmail.com (M. Sadiq), abdennourimohamed@yahoo.fr (M. Abdennouri), barkanoureddine@yahoo.fr (N. Barka)
[b]Laboratoire d'Ingénierie, d'Electrochimie, de Modélisation et d'Environnement (LIEME), Université Sidi Mohamed Ben Abdellah,
Faculté des Sciences Dhar Elmehraz, Fès, Morocco
[c]Laboratoire de Spectro-chimie Appliquée et Environnement (LSCAE), Université Sultan Moulay Slimane,
Faculté des Sciences et Techniques, Béni Mellal, Morocco, email: mahjoubi.fatimazahra@gmail.com
[d]Equipe de Catalyse et Environnement, Département de Chimie, Faculté des Sciences, Université Ibn Zohr, B.P. 8106 Cité Dakhla,
Agadir, Morocco, email: samir_qourzal@yahoo.fr

ABSTRACT

In the present study, natural sand of Merzouga region (NSM) was investigated for the removal of textile dyes from aqueous solutions in static mode. X-ray diffraction analysis, FT-IR spectroscopy, N_2 sorption and transmission electron microscopy were used to investigate physicochemical properties of this siliceous material. The particle size distribution analysis was also used as a simple technique of particle sizing. Characterization of the natural material indicates pure and very fine-sized sand with a weak specific surface area. The effects of solution pH, initial dyes concentration, temperature, contact time and adsorbent dose on the removal of methylene blue (MB) and malachite green (MG) were studied. Results showed that the highest removal efficiency of MB and MG by NSM were performed at basic solution pH. The adsorption of the both dyes followed the pseudo-second-order kinetic model. The thermodynamic parameters obtained demonstrated that MB and MG adsorption process is feasible, spontaneous and endothermic. The equilibrium data were better described by Langmuir isotherm model. In optimal conditions, the maximum adsorption capacities of NSM using Langmuir isotherm model were 1.185 mg/g for MB and 3.144 mg/g for MG. FTIR analysis indicates that the adsorption of MB and MG onto NSM could be done with a physical adsorption. Desorption experiment using deionized water as desorbing agent revealed over 95.32% and 68.98% for MB and MG, respectively.

Keywords: Sand; Adsorption; Desorption; Dyes; Kinetic; Equilibrium

1. Introduction

During the last decades, the rapid industrial development all over the world has generated several pollution sources. Textile processing industries are characterized by their high water consumption and considered one of the major sources of environmental pollutants [1]. The removal of dyes from textile effluents is the most significant environmental problems. Various techniques have been reported for the removal of dyes from industrial effluents and wastewaters that often involve a

* Corresponding author.

combination of different processes to achieve the desired water quality.

Currently, several technologies are available for dyes textile removal from aqueous solution such as photocatalytic degradation [2,3], Fenton's reagent [4], reverse osmosis [5], ion exchange [6], membrane filtration [7] and electrochemical treatment [8]. While, some of these methods are often quite expensive, complex, less sensitive do not generally degrade the pollutant, therefore causing an accumulation of the dye as sludge creating a disposal problem. They have already the limitations of being time-consuming.

For that, special attention is given to the adsorption process [9], because it is one of the efficient, economic and simplest methods for the removal of organic pollutants from aqueous solutions. Therefore, in recent years, considerable attention has been taken, based on economical and environmental concerns, to the investigation of different types of low-cost, easily available and highly effective adsorbents such as activated carbon [10,11], clay [12], hydroxyapatite [13], layered double hydroxides [14], nanocomposite [15,16], starch/poly(alginic acid-cl-acrylamide) nanohydrogel [17], amberlite Ira-938 resin [18] and various biomass materials including *Diplotaxis harra* and *Glebionis coronaria* L. [19], *Trichoderma harzianum* [20], palm kernel [21], *Ziziphus* lotus fruit peels and Avocado kernels seeds [22]. Even though, the research is always, looking for other alternative adsorbents cheaper, abundantly available, as simple and easy to regenerate.

In this context, an available component can be identified, which is the sand. The sand is together small separate mineral grains, recovering the ground. It is identified across to the size grading, the most frequent of its components is the dry quartz and its density varies according to its size grading and its composition. The sand is used as raw material in the glass industry [23], as a filter of liquids and gases [24], as abrasive in factories to clean metallic parts [25], in high-pressure jet to give the effect faded in jeans [26], in agricultural amendment to increase at the same time the pH of an acid ground and improve the texture of lands [27]. The sand is also an element mattering in the tourist domain, when it is present on beaches and dunes. It is little exploited in the field of adsorption of micro-pollutants of the effluents generated by industrial activities.

In this paper, due to its great abundance and physico-chemical properties, the natural sand of Merzouga (NSM) in Morocco was used as adsorbents for dyes removal from the aqueous solutions. Two types of commercial dyes were chosen for this study, including, methylene blue (MB) and malachite green (MG). Adsorption experiments were carried out as a function of solution pH, contact time, adsorbent dosage, initial concentration of dyes and temperature. The kinetics, thermodynamic parameters controlling the adsorption process were also calculated and discussed. Equilibrium sorption isotherms were modeled by Langmuir, Freundlich and Temkin models. The NSM sample was characterized by X-ray powder diffraction, N_2 sorption, FT-IR spectroscopy before and after adsorption and transmission electron microscopy.

2. Experimental methods

2.1. Adsorbent material

NSM was selected as an adsorbent for dyes removal due to its availability and physico-chemical characteristics.

NSM was collected in the dune of Merzouga region in the southeast of Morocco.

2.2. Reagents

All of the reagents used in this study were of analytical grade and were used without any further purification: nitric acid 65% (Scharlau, Spain), sodium hydroxide (Merck, Germany; 98% purity), methylene blue ($C_{16}H_{18}ClN_3S$) and malachite green ($C_{23}H_{25}N_2$) from Sigma-Aldrich Chemical Company, Germany. Characteristics and molecular structures of MB and MG are presented in Table 1. Solutions were prepared with distilled water.

2.3. Procedure and analysis

Natural sand of Merzouga (NSM) was washed, dried at 383 K and calcined at 773 K. Structure, texture, surface morphology and size distribution analyses by sieving were carried out to identify the correlation between the NSM structure and their adsorptive capacity. Several characterization techniques used in this work are described below.
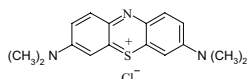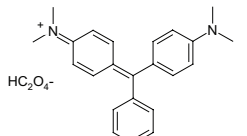
Phases present in the NSM and their crystallinity were determined by performing powder X-ray diffraction (XRD) method. The pattern was scanned from $2\theta = 2°–80°$ at scan rate of 2°/min using a diffractometer (type X'Pert High Score) with Cu Kα radiation. The accelerating voltage and the applied current were 40 kV and 35 mA, respectively.

The specific surface area measurement was carried out by nitrogen adsorption and desorption analysis at 77 K using a Micromeritics Instrument FlowSorb II 2300. Before any measurement was taken, the sample undergoes degassing in 573 K under nitrogen during 4 h to desorbed species on the particles surface.

Infrared absorption spectroscopy spectra were illustrated, after and before adsorption of MB and MG, at room temperature on a Fourier transform infrared spectroscopy (FTIR-2000, PerkinElmer, USA). Before analysis, a small amount of powdered sample was dispersed in a matrix of KBr using weight ratio of (carbon/KBr) = 1/100 and then pressed to form transparent pellet. KBr was previously oven-dried to avoid interferences due to the presence of water and FTIR spectrum was recorded at room temperature in the wavenumbers range of 4,000–400 cm^{-1}.

The microstructure of NSM was observed using transmission electron microscopy (TEM) with a JEM-2010F

Table 1
Physicochemical characteristics of methylene blue and malachite green

Name	Molecular structure	MW (g/mol)	λmax (nm)
Methylene blue (Basic blue 9)		319.85	661
Malachite green (Basic green 4)		329.5	621

microscope (JEOL, France), at an acceleration voltage of 200 kV. The grading analysis by sieving is made on a sample and passed through six sieves.

2.4. Adsorption studies

Stock solutions of dyes were prepared by dissolving desired weight of each dye in distilled water and necessary concentrations were obtained by dilution. Sorption experiments were performed in a series of 50 mL beakers containing the desired weight of NSM and 50 mL of the dye solution at desired concentration. These experiments were carried out at a constant agitation by varying pH of solution from 2 to 10, NSM dosage from 0.5 to 10 g/L, contact time from 0 to 360 min, initial dyes concentration from 10 to 100 mg/L and temperature from 10°C to 50°C. The solution pH was adjusted by adding NaOH (0.1 N) or HNO_3 (0.1 N) and measured by a sensION+ PH31 pH meter. The temperature was controlled using a thermostatically controlled incubator.

After each adsorption experiment completed, the solid phase was separated from the liquid phase by centrifugation at 3,000 rpm for 10 min. Each sample was diluted by distilled water and the residual concentration was determined from its UV–Vis absorbance characteristic with the calibration curve method at the wavelength of maximum absorption at 661 nm for methylene blue and at 621 nm for malachite green. A TOMOS V-1100 model UV-Vis spectrophotometer was used.

The adsorption capacity and adsorption yield were calculated using the following equations:

$$q_e = \frac{(C_o - C)}{R} \tag{1}$$

$$\% \text{ Removal efficiency} = \frac{(C_o - C)}{C_o} \times 100 \tag{2}$$

where q_e is the adsorbed quantity (mg/g), C_0 is the initial dye concentration (mg/L), C is the dye concentration at a time t (mg/L), R is the mass adsorbents per liter of solution (g/L).

Desorption experiment for the NSM was investigated using a desorbing agent. In this study, deionized water was used as an eluent solution to desorb MB and MG from the surface of the NSM. In first time, the adsorption of the both dyes onto NSM was performed for 180 min. The volume of the dye solution was 100 mL with a concentration of 50 mg/L and the weight ratio of 20 g/L. After saturation, the suspension was filtered and the residual solid was contacted with the desorbing solution at the same operating conditions adopted in adsorption. The mixture was stirred for 180 min and then filtered and the concentration of desorbed dye was determined. The percentage of both dyes desorbed was calculated by the following equation:

$$\% \text{ Desorption} = \frac{100 \times C_d}{q_o \times R} \tag{3}$$

where C_d (mg/L) is the concentration of dyes desorbed, q_e (mg/g) is the adsorption capacity of the adsorbent for each dye and R is the weight ratio of the NSM used in desorption.

3. Results and discussion

3.1. Particle size distribution

The grading analysis by sieving is made on a sample of 400.01 g obtained from the source. This sample passed through six sieves. The respective meshings which have six nominal dimensions (*d*): 500, 300, 250, 200, 150 and 100 μm. The masses and the percentages of passing obtained are grouped in Table 2. According to this result, we observe that the particles size was between 200 and 400 μm. It is an average sand according to the classification of Mahaney [28] and Larsonneur [29].

3.2. Characterization

3.2.1. X-ray powder diffraction

Fig. 1 shows the X-ray powder diffraction pattern of NSM sample. Peaks at 2θ = 21°, 27°, 42°, 50° and 60° were

Table 2
Result of the grading test by dry sieving

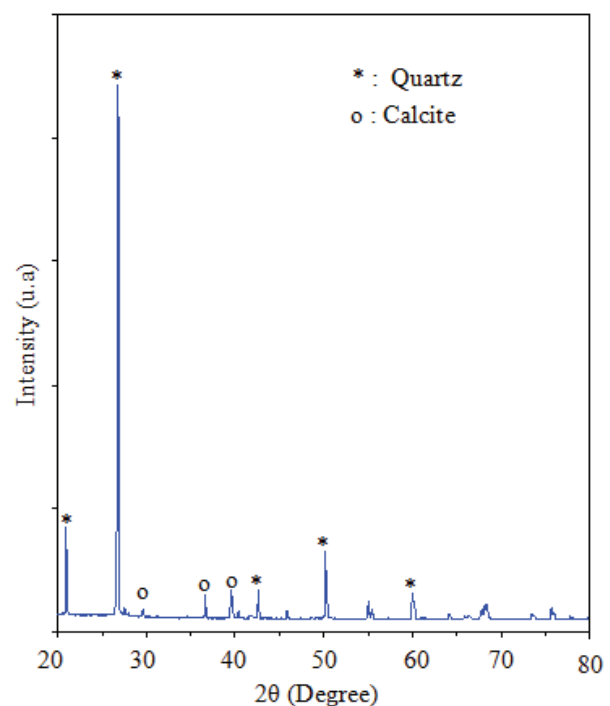| *d* (μm)	Retained (g)	Cumulative retained (g)	Passing (g)	% Passing
0	400.01	400.01	0	0
100	5.37	393.51	6.5	1.62
150	22.23	388.14	11.87	2.97
200	61.05	365.91	34.10	8.52
250	105.45	304.86	95.15	23.79
300	199.41	199.41	200.6	50.15
500	0	0	400.01	100

Fig. 1. X-ray diffraction pattern of the NSM.

attributed to the quartz phase. The peaks observed at $2\theta = 29°$, $36°$ and $39°$ are attributed to the crystalline calcite phase. The fineness peaks indicate that the NSM was well crystallized. This result indicated that the sand of dune of Merzouga is siliceous sand.

3.2.2. Specific surface area determination

The specific surface area calculated from the classic formula of Brunauer–Emmet–Teller of the NSM was estimated as 2.7 m^2/g. This small surface area suggested that the NSM do not have relatively defined holes on their surface.

3.2.3. Transmission electron microscopy observation

Fig. 2 presents the TEM particle morphologies of the NSM studied in different size grading between 150 and 500 μm. In this surface, particles possess a uniform distribution. The images (a, b), (c, d), (e, f) and (g, h) correspond, respectively, in size grading $150 < d < 200$ μm, $200 < d < 250$ μm, $250 < d < 300$ μm and $300 < d < 500$ μm. Images b, d, f and h show that size on this studied sand are in varied forms. This can be explained by coming from distant regions under the effect of the wind. Figs. 2(a), (c), (e) and (g) show the existence of black small points corresponding to the spaces of pore as holes on the surface which looks similar to a sponge. This wide porous texture is a very good argument showing the capacity of adsorption of this sand.

4. Adsorption study

4.1. Effect of solution pH

The adsorption process is mostly affected by the variation in solution pH. In general, the effect of solution pH depends on the ions present in the reaction mixture and then on the electrostatic interactions with the surface of the adsorbent. Both aqueous chemistry and surface binding sites of the adsorbents are influenced by solution pH. The effect of the variation of solution pH on the adsorption of MB and MG onto NSM is illustrated in Fig. 3. The figure indicates that MB sorption decreases with the increase of solution pH from 4 to 9; as a result, the removal efficiency decreases from 62% to 44%. For pH values between 9 and 12, the removal efficiency of the dye increased gradually. For MG, the adsorption efficiency increased simultaneously with increasing solution pH from 6 to 9. The highest adsorption yield of MB and MG were obtained at basic pH solution. This is due to the fact that, with the increase of solution pH, the surface of the adsorbent particles becomes negatively charged. Consequently the ionic absorbent–adsorbate interaction with cationic dyes (MB and MG) becomes progressively significant. Hence, basic medium pH was suitable for the removal of 65% of MB and 93% of MG onto NSM.

4.2. Effect of adsorbent dosage

Optimum adsorbent dosage is one of the important parameters to be studied. It gives information on the amount of adsorbate adsorbed as a function of the number of available adsorption sites and the surface area increases by increasing the adsorbent dosage. The removal efficiency of MB and MG by NSM are shown in Fig. 4. The figure shows that the adsorbent yield of the both dyes increases with increasing the adsorbent dosage and maximum removal efficiency occurs at an adsorbent dosage of 30 g/L. This variation can be justified by the availability of more number of sorption sites on the surface of the sand. From the figure, it could be seen that 30 g/L of sand is sufficient to remove about 80% of MG and 50% of MB. The sorption yield of MG is greater than that of MB. This difference may be due to the nature of adsorbent–adsorbate interactions.

4.3. Adsorption kinetics

The kinetic study presents a major parameter on the process of adsorption. Fig. 5 illustrates the effect of contact time on the adsorption of MB and MG on the NSM. Kinetics data of solute uptake is required for selecting optimum conditions for full-scale with batch process. From the figure, it could be seen that the adsorption of MB and MG were rapid at the first period of the process and it accuses equilibrium after about 240 min. In fact, values of adsorbed quantity (q) were increased quickly, and after 240 min they become almost constant. This time can be considered optimal for effective retention of the both dyes onto NSM. The kinetic data were analyzed by different kinetic models: pseudo-first order, pseudo-second order equations and the intraparticle diffusion model. The obtained results are, respectively, illustrated in Figs. 6–8.

The first-order rate expression of Lagergren based on solid capacity is generally expressed as follows [30]:

$$q = q_e\left(1 - e^{-k_1 t}\right) \tag{4}$$

where q_e and q (both in mg/g) are, respectively, the amounts of dye adsorbed at equilibrium and at any time t (min), and k_1 (1/min) is the rate constant of adsorption.

The pseudo-second order model proposed by Ho and McKay [31] is based on the assumption that the sorption follows second order chemisorption. The pseudo-second order model can be expressed as:

$$q = \frac{k_2 q_e^2 t}{1 + k_2 q_e t} \tag{5}$$

where k_2 (g/mg min) is the rate constant of pseudo-second order adsorption.

In order to explain the diffusion mechanism, the intraparticle diffusion model was used. This model explains a multi-step kinetic sorption process. In general, however, the external diffusion can be considered negligible; especially in well stirred system [32], the rate controlling step is the intraparticle diffusion step. The equation of the intraparticle diffusion kinetic model is expressed as follows [33]:

$$q = K_i t^{0.5} + l \tag{6}$$

where q is the amount of solute adsorbed at any time (mg/g); K_i (mg/K min$^{1/2}$) is the adsorption rate constant, and l is the
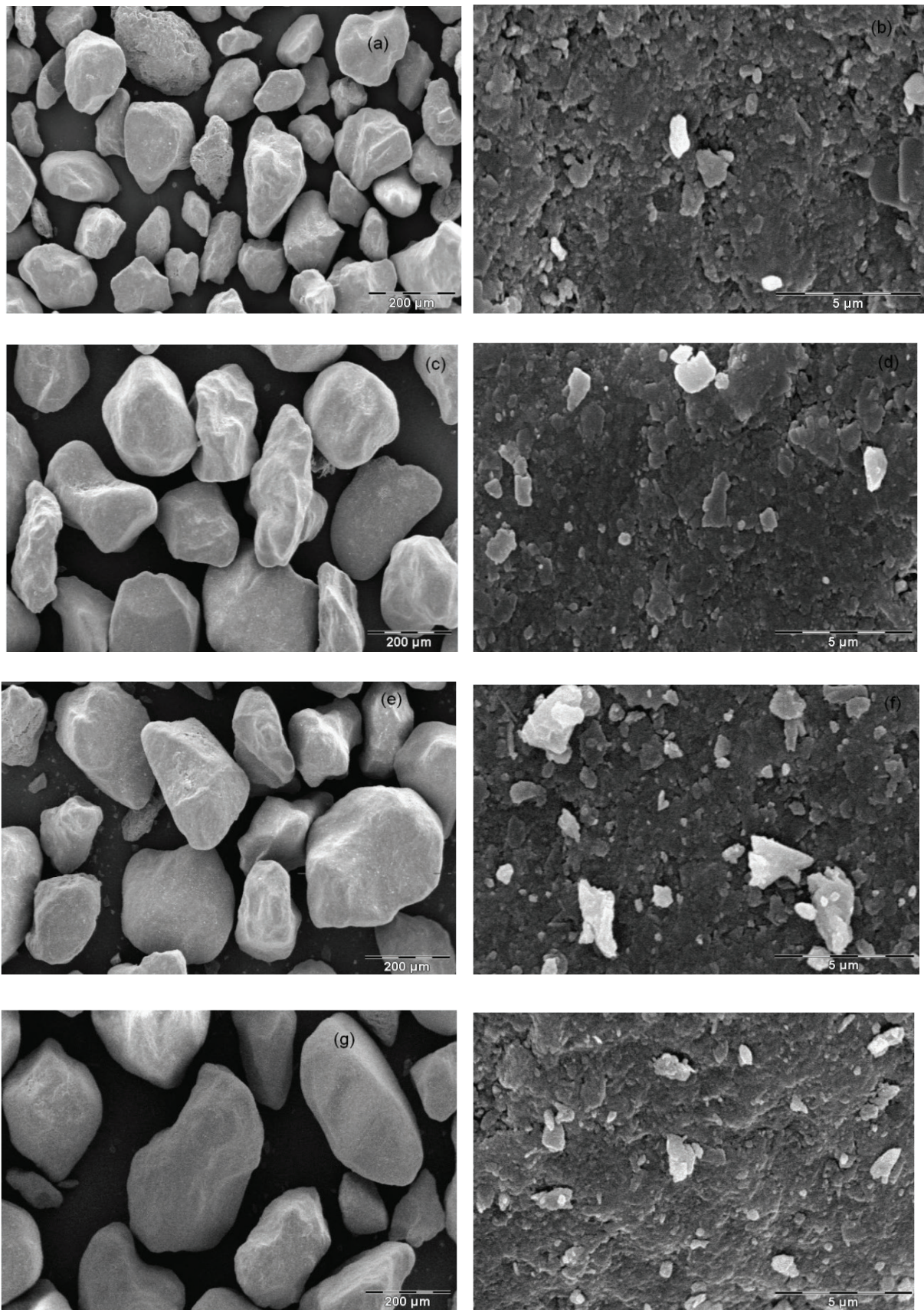
Fig. 2. TEM micrographs of NSM.

effect of boundary layer thickness. The K_i values can be determined through a linear regressions of q vs. $t^{0.5}$ [32].

The validity of each model was tested by estimating the correlation coefficient, r^2 value and sorption capacity (q_{exp}). Parameters of the pseudo-first order and pseudo-second order models were evaluated with the aid of the non-linear regression using Origin 6.0 software. All relative parameters
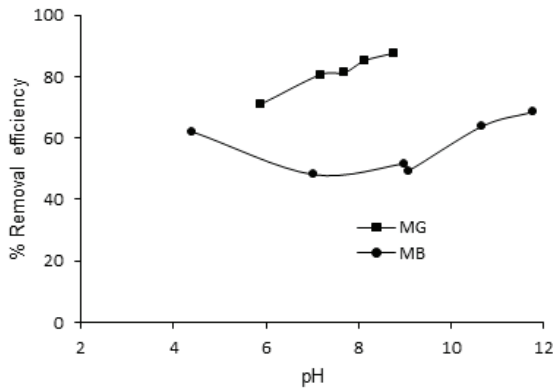

Fig. 3. Effect of pH on the adsorption of MB and MG onto NSM: C_0 = 50 mg/L, R = 40 g/L, time = 180 min, T = 25°C.
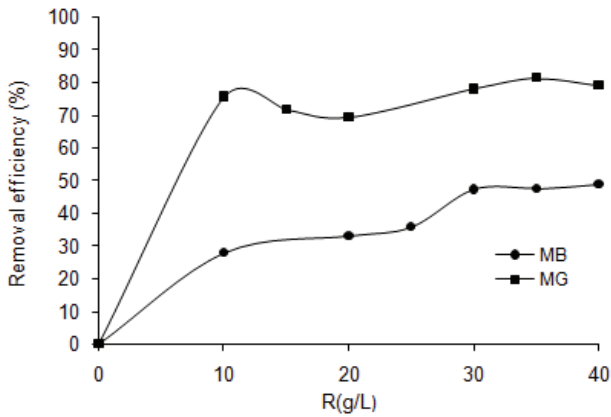

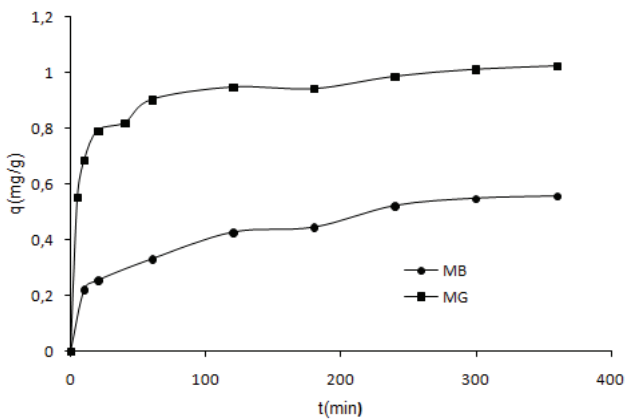Fig. 4. MB and MG removal efficiency as function of NSM dose: C_0 = 50 mg/L, time = 180 min, T = 25°C.

Fig. 5. Kinetics of adsorption of MB and MG by NSM: C_0 = 50 mg/L, R = 40 g/L, T = 25°C.

Fig. 6. Comparison between fitted curves by pseudo-first order, pseudo-second order kinetics models and the experimental points of MB adsorption.
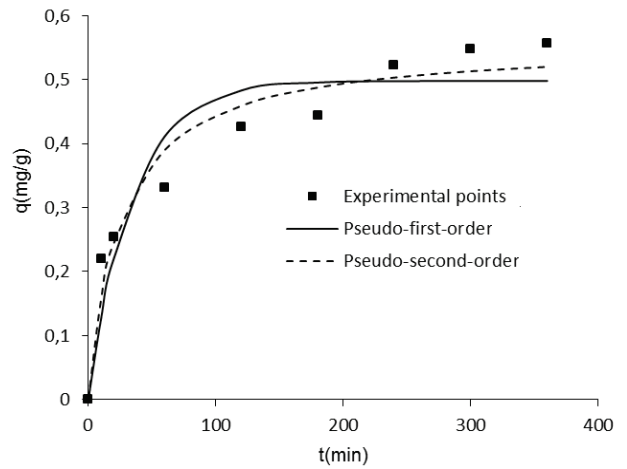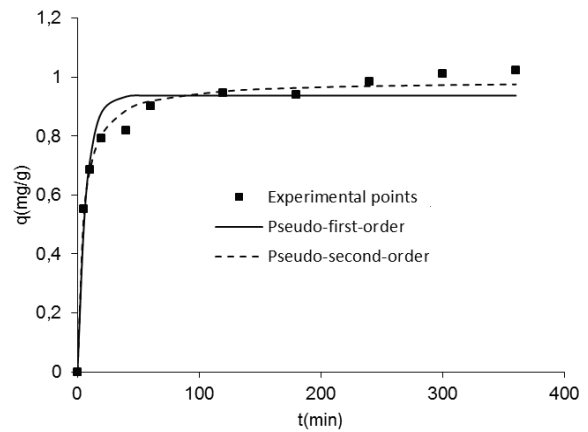

Fig. 7. Comparison between fitted curves by pseudo-first order, pseudo-second order kinetics models and the experimental points of MG adsorption.
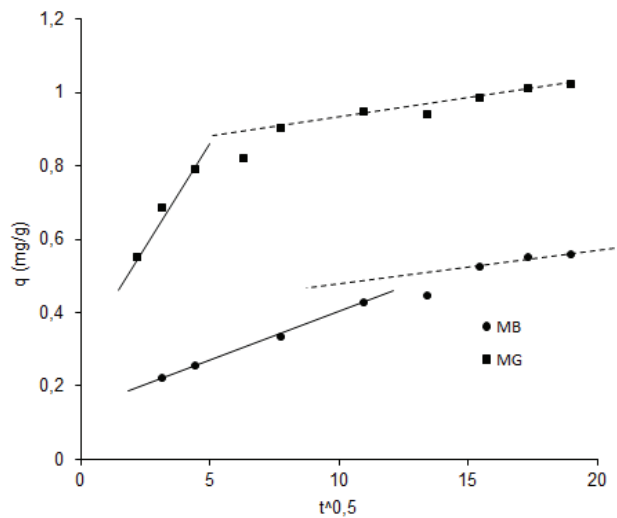

Fig. 8. Intraparticle diffusion of MB and MG by NSM.

Table 3
Kinetic constant values for MB and MG adsorption onto NSM

Dyes		MB	MG
Pseudo-first order	q_{exp} (mg/g)	0.557	0.940
	q_{cal} (mg/g)	0.557	0.987
	k_1 (1/min)	0.029	0.141
	r^2	0.893	0.950
Pseudo-second order	q_{cal} (mg/g)	0.498	0.937
	k_2 (g/mg min)	0.069	0.223
	r^2	0.950	0.988
Intraparticle diffusion	K_i (mg/K min$^{1/2}$)	<0.0001	0.029
	L	9	11
	r^2	0.937	0.652

Fig. 9. Effect of temperature on the adsorption of MB and MG onto NSM: C_0 = 50 mg/L, R = 40 g/L, time = 180 min.

of the pseudo-first order, pseudo-second order kinetic and the intraparticle diffusion model are listed in Table 3. The table shows that, for MB and MG sorption, the values of correlation coefficient were closer to 1 in the case of pseudo-second order than pseudo-first order model. Although, the calculated equilibrium values (q_{cal}) from pseudo-second order model were more compatible with the experimental equilibrium values (q_{exp}) than the others calculated from the pseudo-first-order model for the both dyes.

In fact, in the intraparticle diffusion model, the dye adsorption by NSM involves several steps, which are: transfer of dye from the solution to the adsorbent surface, film diffusion, dye adsorption on the outer surface of the adsorbent, dye diffusion in the pores and in the solid phase (intraparticle diffusion), and finally, dye adsorption on the active sites in the interior surface of the adsorbents [34]. From the plot of q_t versus $t^{0.5}$, the values of intraparticle diffusion rate constant (k_i) and the effect of boundary layer thickness (l) were calculated (Table 3). As shown from Fig. 8 that the plots are not more linear through all the time ranges for the both dyes. While, the correlation coefficient in the case of MB sorption indicate a value close to 1 than this one in MG, which means that the adsorption process is not governed principally by intraparticle diffusion. If the intercept length increased, adsorption is more boundary layer controlled.

The analysis of these results shows that the adsorption of MB and MG could be more described by the pseudo-second order model. These results provide that the adsorption capacity may be due to the higher driving force making the transfer of MB and MG molecules to the surface of the adsorbent particles.

4.4. Effect of temperature

The effect of temperature on the adsorption of dyes is very important in the real application of adsorption as various textile and other dyes effluent produced at relatively different temperatures. Indeed, it promotes the diffusion of molecules across the external boundary layer and the internal pores of the adsorbent particles, probably due to the decrease of the viscosity of the solution. Fig. 9 represents the variation of the percentage sorption of MB and MG on the NSM as function of the temperature. The curves indicate that the temperature has a less significant effect on the adsorption of both the dyes
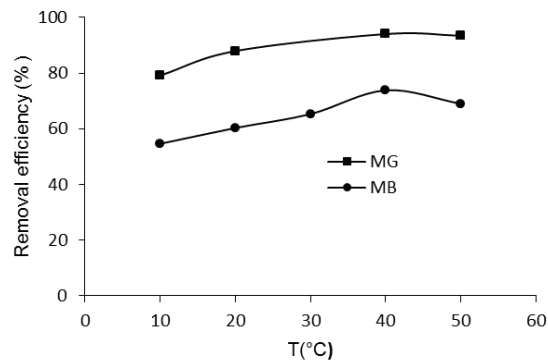
onto NSM. It is found that the removal efficiency of the MB and MG slightly increases in the temperature range between 10°C and 50°C. It also appears that the adsorption of MG is important than MB. The relatively small surface area may be explaining the obtained result.

Thermodynamic parameters including the change in free energy ($\Delta G°$), enthalpy ($\Delta H°$) and entropy ($\Delta S°$) were used to describe thermodynamic behavior of the adsorption of MB and MG onto NSM. These parameters were evaluated to discover the spontaneous nature and the changes in randomness of the system. Then, the exothermic or endothermic nature of the adsorption process can be also determined.

These thermodynamic parameters were determined according the following reversible process [35]:

$$\text{dye in solution} \rightleftharpoons \text{adsorbed dye} \qquad (7)$$
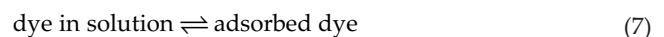
For such equilibrium reactions, K_D, the distribution constant, can be expressed as:

$$K_D = \frac{q_e}{C_e} \qquad (8)$$

The Gibbs free energy ($\Delta G°$) was calculated using the following equation:

$$\Delta G° = -RT\ln(K_D) \qquad (9)$$

where R is the universal gas constant (8.314 J mol/K) and T is solution temperature in K.

The enthalpy ($\Delta H°$) and entropy ($\Delta S°$) of adsorption were estimated from the slope and intercept of the plot of $\ln K_D$ vs. $1/T$ yields, respectively. They were determined using van't Hoff equation:

$$\text{Ln}K_D = -\frac{\Delta G°}{RT} = -\frac{\Delta H°}{RT} + \frac{\Delta S°}{R} \qquad (10)$$

Thermodynamic parameters calculated for the adsorption of MB and MG onto NSM are illustrated in Table 4. It could be seen from this table that the adsorption of dyes is thermodynamically favorable with a spontaneous adsorption

process due to the negative values of Gibbs free energy ($\Delta G°$) at different temperature [36,37]. As shown that the enthalpy of adsorption ($\Delta H°$) is of the order of 0.0025 kJ/mol for MB and 0.0016 kJ/mol for MG, these positive values indicate that the adsorption is endothermic [38]. The $\Delta S°$ parameter was found to be positive for adsorption of MB and MG onto NSM proving an increase in the randomness at the solid/solution interface during the adsorption [39].

4.5. Adsorption isotherms

Adsorption isotherms are important in this study as they describe the possible interaction between the adsorbate and adsorbent. The equilibrium adsorption capacities vs. concentrations of the dye solution at equilibrium are represented in Figs. 10 and 11. It could be seen from these figures that the equilibrium adsorption capacity increases with the increasing of initial concentration of dyes. The increase in adsorbed amounts with concentration is probably due to a high driving force for mass transfer. Hence, high concentration in solution implicates greater amount of dye molecules fixed at the surface of NSM. To explain more the adsorption process, the obtained equilibrium data were modeled using different isotherm models. In this study, three adsorption equilibriums isotherm models including Langmuir, Freundlich

Table 4
Thermodynamic parameters calculated for the adsorption of MB and MG onto NSM

Adsorbent		NSM				
Adsorbate	T (°C)	q_e (mg/g)	K_D	$\Delta G°$ (J/mol)	$\Delta H°$ (kJ/mol)	$\Delta S°$ (J/K mol)
MB	10	0.66	0.03	–5,414.45	0.0025	0.02
	20	0.73	0.07	–4,167.69	0.0025	0.02
	40	0.90	0.07	–2,447.31	0.0025	0.02
	50	0.84	0.05	–2,821.00	0.0025	0.02
MG	10	1.02	0.10	–8,239.38	0.0016	0.02
	20	1.13	0.18	–6,458.71	0.0016	0.02
	40	1.21	0.39	–6,899.35	0.0016	0.02
	50	1.20	0.35	–8,033.14	0.0016	0.02

and Temkin models have been used for the analysis of the obtained equilibrium data.

4.5.1. Langmuir isotherm

The Langmuir isotherm assumes that sorption comes from the monolayer coverage of adsorbate over a homogenous adsorbent surface [40]. This model supposes that sorption occurs on specific homogeneous sites within the adsorbent and all its sorption sites are energetically identical. The mathematical expression of the Langmuir isotherm is given by Eq. (11):

$$q_e = \frac{q_m K_L C_e}{1 + K_L C_e} \tag{11}$$

where q_m (mg/g) is the maximum monolayer adsorption capacity and K_L (L/mg) is the Langmuir equilibrium constant related to the sorption affinity. C_e is the equilibrium concentration.

4.5.2. Freundlich isotherm

The Freundlich isotherm is an empirical model of heterogeneous surface sorption with non-uniform distribution of heat sorption and affinities [41]. It is expressed mathematically by Eq. (12):

$$q_e = K_F C_e^{1/n} \tag{12}$$

where K_F (mg$^{1-1/n}$/g L$^{1/n}$) and n are Freundlich constants. n is the heterogeneity factor related to adsorption affinity and K_F is related to the adsorption capacity.

If the values of n are in the range of 1–10, it can be considered that the sorption process indicates a favorable and slightly difficult sorption. However, the sorption is very insignificant when n is lower than 1. Also, if the value of n is equal to unity, the adsorption is linear; if the value is below to unity, it can be deduced that sorption process is chemical, if the value is above unity adsorption is a favorable physical process.
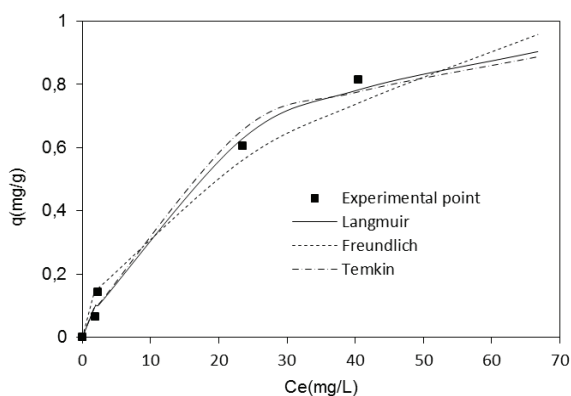

Fig. 10. Experimental points and fitted isotherm curves for MB adsorption onto NSM.
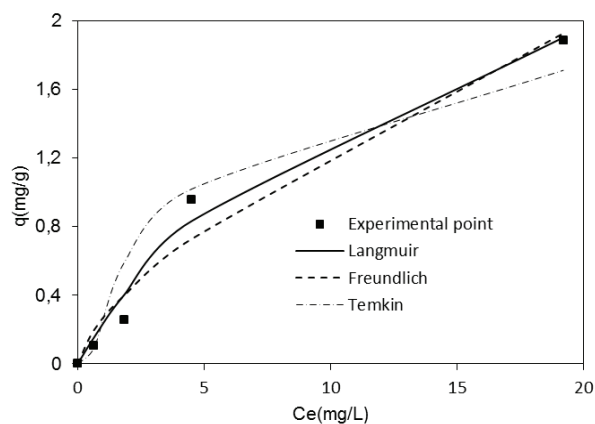

Fig. 11. Experimental points and fitted isotherm curves for MG adsorption onto NSM

4.5.3. Temkin isotherm

Temkin isotherm model suggests a uniform distribution of binding energies and assumes the effects of the interaction of the adsorbate and the adsorbing species [42]. This isotherm assumes that the heat of adsorption of all the molecules in the layer would decrease linearly rather than logarithmically with coverage owing to adsorbate–sorbent interactions. The Temkin isotherm has been expressed mathematically as:

$$q_e = B \ln(K_T C_e) \tag{13}$$

where $B = RT/b$, T (K) is the absolute temperature and R is the universal gas constant (8.314 J/mol).

B is the Temkin constant related to the heat of adsorption (kJ/mol), and K_T empirical Temkin constant related to the equilibrium binding constant related to the maximum binding energy (L/mg).

The calculated results from the curves of Langmuir, Freundlich and Temkin isotherm models for MB and MG have been summarized in Table 5. The higher values of r^2 accused the applicability of the Langmuir model for dyes sorption onto the NSM. Therefore, the best fit of experimental data was obtained with the Langmuir model. For the Freundlich model, the correlation coefficients are lower. The values of $n > 1$ indicated favorable adsorption at experimental conditions of the both dyes sorption onto NSM. The Temkin model found a calculation about equilibrium binding constant corresponding to the maximum binding energy, K_T. This model presents a correlation coefficient $r^2 > 0.98$ for the MB sorption and a lower value in the case of MG sorption. The comparison between the three models for the analysis of optimization data provides that the Langmuir model is the most suitable to fit the adsorption data.

On the other hand, it appears that the removal efficiency of the sand was independent to the specific surface. It was so due to the interactions between functional groups at the sand surface and groupements of dyes. These interactions could be considered as links of van der Waals nature. This is seen in the equilibrium data that it was fitted to the Langmuir model.

Maximum adsorption capacity obtained from the removal of MB and MG onto NSM was compared with the previous records of various low-cost adsorbent as summarized in Table 6. It can be observed that experimental data of the present study were found to be higher than those of some corresponding adsorbents in the literature.

4.6. Contribution of functional groups in the sorption

Fig. 12 shows FT-IR spectra of NSM sample before and after adsorption of both the dyes. From the FTIR spectra, the observed changes occurring on the NSM after adsorption of MB and MG are reflected in the broad and strong bands at 3,436 and 1,617 cm⁻¹, which are attributed to the stretching and bending of hydroxyls vibrations of Mg-OH and Fe-OH groups, respectively. The bands situated at 1,418 and at 693 cm⁻¹ are assigned to the stretching vibration modes characteristic of the groupings of carbonates. The bands situated in 1,080 cm⁻¹, that divided into two at 796 and at 778 cm⁻¹ and at 459 cm⁻¹ are, respectively, bending in the plane and outside the plane of the groupings silicon–oxygen. The intensity of bands around 1,080 cm⁻¹ confirms that the sand of Merzouga is very rich in silica. This result is in accordance with X-ray diffraction result.

Table 5
Equilibrium constant values for MB and MG onto NSM

Dyes	Langmuir			Freundlich			Temkin		
	q_m (mg/g)	K_l (L/mg)	r^2	n	K_f (mg$^{1-1/n}$/g/L^n)	r^2	K_t (L/mg)	B (kJ/mol)	r^2
MB	1.185	0.047	0.992	1.949	0.111	0.974	0.822	0.221	0.985
MG	3.144	0.079	0.984	1.488	0.264	0.967	1.869	0.478	0.918

Table 6
Comparison of maximum adsorption capacity of NSM for MB and MG with different adsorbents

| Adsorbent	q (mg/g) MB	q (mg/g) MG	References
Raw KT3B kaolin (Algeria)	52.76	–	[43]
Kaolinite	102.04	–	[44]
Nanoporous activated carbon prepared from karanj	154.8	–	[45]
Polyaniline nanotubes (PANI NTs)	09.21	–	[46]
Graphene oxide nanosheets (GO) at 25°C	03.57	–	[47]
Graphene oxide nanosheets (GO) at 35°C	4.37	–	[47]
Activated lignin–chitosan extruded (ALiCE)	36.25	–	[48]
Almond gum	–	196.07	[49]
Chitosan ionic liquid beads A (1-butyl-3-methylimidazolium acetate A)	–	08.07	[50]
Chitosan ionic liquid beads B (1-butyl-3-methylimidazolium chloride B)	–	0.24	[50]
Natural zeolite	–	4.15×10^{-5}	[51]
Natural sand of Morocco (NSM)	1.185	3.144	This study
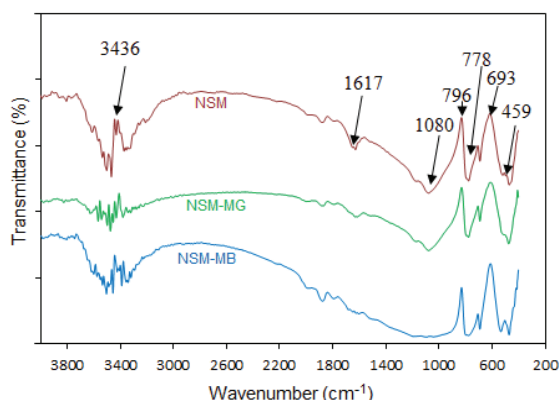
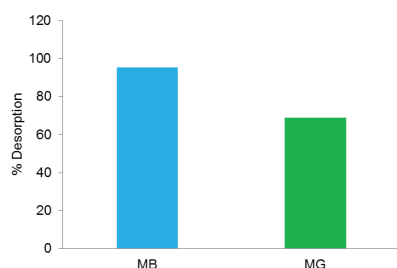Fig. 12. FT-IR spectra of the NSM before and after adsorption of MB and MG.

Fig. 13. Percentages of MB and MG desorbed from loaded NSM using deionized water.

After loading of MB and MG, the FTIR spectra demonstrate some shifts of the wavenumber of hydroxyl groups. Hence, before and after adsorption of both the dyes, the infrared spectrum indicated no chemical change on the majority of functional groups of NSM, which suggested that the adsorption of MB and MG onto NSM could be done with a physical adsorption [52].

4.7. Desorption of MB and MG from NSM

Disposal of an adsorbent loaded with textile dyes creates another environmental problem and requires further treatment. For this reason, regeneration of adsorbent materials through desorption of the dyes is of crucial importance. The desorption process is also important in order to recover the adsorbed dyes for reuse. Fig. 13 presents the percentages of MB and MG desorbed from loaded NSM using deionized water. The figure indicates that the desorbed percentages of MB and MG were found to be 95.32% and 68.98%, respectively. These results indicate that distilled water is fairly efficient at desorbing the adsorbed MB and MG onto NSM.

5. Conclusion

This work focused on the study of the elimination of textile dyes by adsorption on the sand of Merzouga. Experimental results show that the adsorption process depends on the pH of dye solution, of the concentration and of the mass of adsorbent. The amount of adsorption of methylene blue and malachite green in the NSM increases with increasing of the basicity of

the solution. Therefore, very significant sorption efficiency was achieved in basic medium. The kinetic study of the adsorption of MG and MB onto NSM showed that the adsorption process was initially rapid and then slowed down until reaching the equilibrium to 240 min. The kinetics of adsorption of MG and MB was better described by the pseudo-second order. For the effect of dosage sorbent, a mass ratio of 40 g/L is sufficient to remove about 80% of MG and 50% of MB. The thermodynamic parameters obtained at different temperature indicate that MB and MG adsorption onto NSM process is spontaneous and endothermic. Further, equilibrium isotherms of both the dyes were more described adequately by the Langmuir isotherm model. The optimization of the parameters influencing the dyes sorption shows that the adsorption efficiency of the malachite green was greater than that of methylene blue.

Sand of Merzouga proved as an adsorbent having a relatively average adsorption affinity of textile dyes. Nevertheless, the natural abundance of this material can offer a new adsorbent for wastewater treatment. In addition, the easy desorption of sand adds an advantage in using this material for the adsorption of textile dyes.

References

[1] A. Hasanbeigi, L. Price, A technical review of emerging technologies for energy and water efficiency and pollution reduction in the textile industry, J. Clean. Prod., 95 (2015) 30–44.

[2] A. Abaamrane, S. Qourzal, N. Barka, S. Mançour-Billah, A. Assabbane, Y. Ait-Ichou, Optimal decolorization efficiency of indigo carmine by TiO$_2$/UV photocatalytic process coupled with response surface methodology, Orient. J. Chem., 28 (2012) 1091–1098.

[3] D. Pathania, R. Katwal, G. Sharma, Mu. Naushad, M.R. Khan, A.H. Al-Muhtaseb, Novel guar gum/Al$_2$O$_3$ nanocomposite as an effective photocatalyst for the degradation of malachite green dye, Int. J. Biol. Macromol., 87 (2016) 366–374.

[4] P.V. Nidheesh, R. Gandhimathi, S.T. Ramesh, Degradation of dyes from aqueous solution by Fenton processes: a review, Environ. Sci. Pollut. Res. Int., 20 (2013) 2099–2132.

[5] V. Colla, T.A. Branca, F. Rosito, C. Lucca, B.P. Vivas, V.M. Delmiro, Sustainable Reverse Osmosis application for wastewater treatment in the steel industry, J. Clean. Prod., 130 (2016) 103–115.

[6] G. Darmograi, B. Prelot, A. Geneste, L.C. Menorval, J. Zajac, Removal of three anionic orange-type dyes and Cr(VI) oxyanion from aqueous solutions onto strongly basic anion-exchange resin. The effect of single-component and competitive adsorption, Colloids Surf. A, 508 (2016) 240–250.

[7] J. Lin, W. Ye, M.C. Baltaru, Y.P. Tang, N.J. Bernstein, P. Gao, S. Balta, M. Vlad, A. Volodin, A. Sotto, P. Luis, A.L. Zydney, B.V. Bruggen, Tight ultrafiltration membranes for enhanced separation of dyes and Na$_2$SO$_4$ during textile wastewater treatment, J. Membr. Sci., 514 (2016) 217–228.

[8] F.C. Moreiraa, R.A.R. Boaventuraa, E. Brillas, V.J.P. Vilar, Electrochemical advanced oxidation processes: a review on their application to synthetic and real wastewaters, Appl. Catal. B, 202 (2017) 217–261.

[9] N. Barka, A. Assabbane, Y. Ichou, A. Nounah, Decantamination of textile wastewater by powdered activated carbon, J. Appl. Sci., 6 (2006) 692–695.

[10] N. Sivarajasekar, N. Mohanraj, R. Baskar, S. Sivamani, Fixed-bed adsorption of ranitidine hydrochloride onto microwave assisted-activated aegle marmelos correa fruit shell: statistical optimization and breakthrough modelling, Arabian J. Sci. Eng., 5 (2018) 2205–2215.

[11] N. Sivarajasekara, N. Mohanrajb, K. Balasubramanic, J. Prakash Marand, I. Ganesh Moorthye, V. Karthikf , K. Karthikeyan, Optimization, equilibrium and kinetic studies on ibuprofen

removal onto microwave assisted – activated *Aegle marmelos* correa fruit shell, Desal. Wat. Treat., 84 (2017) 48–58.

[12] A. Kausar, M. Iqbal, A. Javed, K. Aftab, Z.H. Nazli, H.N. Bhatti, S. Nouren, Dyes adsorption using clay and modified clay: a review, J. Mol. Liq., 256 (2018) 395–407.

[13] W. Lemlikchi, N. Drouiche, N. Belaicha, N. Oubagha, B. Baaziz, M.O. Mecherri, Kinetic study of the adsorption of textile dyes on synthetic hydroxyapatite in aqueous solution, J. Ind. Eng. Chem., 32 (2015) 233–237.

[14] F.Z. Mahjoubi, A. Khalidi, M. Abdennouri, N. Barka, M-Al-SO$_4$ layered double hydroxides (M=Zn, Mg or Ni): synthesis, characterization and textile dyes removal efficiency, Desal, Wat. Treat., 57 (2016) 21564–21576.

[15] A.A. Alqadami, Mu. Naushad, M.A. Abdalla, M.R. Khan, Z.A. Alothman, Adsorptive removal of toxic dye using Fe$_3$O$_4$–TSC nanocomposite: equilibrium, kinetic, and thermodynamic studies, J. Clean. Prod., 52 (2017) 443–453.

[16] G. Sharma, Mu. Naushad, D. Pathania, A. Kumar, A multifunctional nanocomposite pectin thorium(IV) tungstomolybdate for heavy metal separation and photoremediation of malachite green, Desal. Wat. Treat., 57 (2016) 19443–19455.

[17] G. Sharma, Mu. Naushad, A. Kumar, Sh. Rana, Sh. Sharma, A. Bhatnagar, F.J. Stadler, A.A. Ghfar, M.R. Khan, Efficient removal of coomassie brilliant blue R-250 dye using starch/poly(alginic acid-cl-acrylamide) nanohydrogel, Process Saf. Environ. Prot., 109 (2017) 301–310.

[18] Mu. Naushad, Z.A. ALOthman, M.R. Awual, S.M. Alfadul, T. Ahamad, Adsorption of rose Bengal dye from aqueous solution by amberlite Ira-938 resin: kinetics, isotherms, and thermodynamic studies, Desal. Wat. Treat., 57 (2016) 13527–13533.

[19] H. Tounsadi, A. Khalidi, M. Abdennouri, N. Barka, Potential capability of natural biosorbents: *Diplotaxis harra* and *Glebionis coronaria* L. on the removal efficiency of dyes from aqueous solutions, Desal. Wat. Treat., 57 (2016) 16633–16642.

[20] V. Karthik, K. Saravanan, N. Sivarajasekar, N. Suriyanarayanan, Utilization of biomass from *Trichoderma harzianum* for the adsorption of reactive red, dye, Environ. Conserv., 22 (2016) S435–S440.

[21] S. Ming-Twang, M.A.A. Zaini, L.M. Salleha, M. Azizi Che Yunusa, M. Naushad, Potassium hydroxide-treated palm kernel shell sorbents for the efficient removal of methyl violet dye, Desal. Wat. Treat., 84 (2017) 262–270.

[22] A. Machrouhi, A. Elhalil, M. Farnane, F.Z. Mahjoubi, H. Tounsadi, M. Sadiq, M. Abdennouri, N. Barka, Adsorption behavior of methylene blue onto powdered *Ziziphus* lotus fruit peels and Avocado kernels seeds, J. Appl. Surf. Interface, 1 (2017) 49–56.

[23] D. Brems, P. Degryse, F. Hasendoncks, D. Gimeno, A.S.E. Vassilieva, S. Luypaers, J. Honing, Western Mediterranean sand deposits as a raw material for Roman glass production, J. Archaeol. Sci., 39 (2012) 2897–2907.

[24] J. Yang, L. Zhao, Wastewater Treatment Performance of Earthworm Biofilter with Filter Media of Quartz Sand and Ceramic Pellet, 2nd International Conference on Bioinformatics and Biomedical Engineering, Shanghai, China, 2008.

[25] X. Ji, J. Zha, X. Zhang, M. Zhou, Erosion–corrosion behavior of Zr-based bulk metallic glass in saline-sand slurry, Tribol. Int., 60 (2013) 19–24.

[26] C.W. Kan, Washing Techniques for Denim Jeans, Denim, 2015, pp. 313–356.

[27] N.L. Ukwattage, P.G. Ranjith, M. Bouazza, The use of coal combustion fly ash as a soil amendment in agricultural lands (with comments on its potential to improve food security and sequester carbon), J. Fuel, 109 (2013) 400–408.

[28] W.C. Mahaney, Atlas of Sand Grain Surface Textures and Applications, Oxford University Press, Oxford, 2002.

[29] C. Larsonneur, La cartographie des dépôts meubles sur le plateau continental français: méthode mise au point et utilisée en Manche. J. Recherche Océanographique, II (1977) 33–39.

[30] S. Lagergren, About the theorie of so-called adsorption of soluble substance, K. Sven. Vetensk.akad. Handl., 24 (1898) 1–39.

[31] Y.S. Ho, G. Mckay, The kinetics of sorption of basic dyes from aqueous solution by sphagnum mass peat, Can. J. Chem. Eng., 76 (1998) 822–827.

[32] G. McKay, V. Poots, Kinetics and diffusion processes in colour removal from effluent using wood as an adsorbent, J. Chem. Technol. Biotechnol., 30 (1980) 279–292.

[33] J. Crank, The Mathematics of Diffusion, Clarendon Press, Oxford, 1979.

[34] W. Plazinski, W. Rudzinski, A. Plazinska, Theoretical models of sorption kinetics including a surface reaction mechanism: a review, Adv. Colloid Interface Sci., 152 (2009) 2–13.

[35] O.M. Paska, C. Pacurariu, S.G. Muntean, Kinetic and thermodynamic studies on methylene blue biosorption using corn-husk, RSC Adv., 4 (2014) 62621–62630.

[36] A.L. Nashine, A.R. Tembhurkar, Equilibrium, kinetic and thermodynamic studies for adsorption of As(III) on coconut (*Cocos nucifera* L.) fiber, J. Environ. Chem. Eng., 4 (2016) 3267–3273.

[37] I. Anastopoulos, G.Z. Kyzas, Are the thermodynamic parameters correctly estimated in liquid-phase adsorption phenomena?, J. Mol. Liq., 218 (2016) 174–185.

[38] S.G. Muntean, A. Todea, S. Bakardjieva, C. Bologa, Removal of non benzidine direct red dye from aqueous solution by using natural sorbents: beech and silver fir, Desal. Wat. Treat., 66 (2017) 235–250.

[39] D. Robati, B. Mirza, M. Rajabi, O. Moradi, I. Tyagi, S. Agarwal, V.K. Gupta, Removal of hazardous Dyes-BR 12 and methyl orange using graphene oxide as an adsorbent from aqueous phase, Chem. Eng. J., 284 (2016) 687–697.

[40] I. Langmuir, The constitution and fundamental properties of solids and liquids, J. Am. Chem. Soc., 38 (1916) 2221–2295.

[41] H. Freundlich, W. Heller, The adsorption of cis- and trans-azobenzene, J. Am. Chem. Soc., 61 (1939) 2228–2230.

[42] M.J. Temkin, V. Pyzhev, Kinetics of ammonia synthesis on promoted iron catalysts, Acta Physicochim., URSS, 12 (1940) 217–222.

[43] M. Lotfi, L. Belkhiri, J.-C. ollingerc, A. Bouzazad, A. Assadid, A. Tirrib, F. Dahmounee, K. Madanie, H. Remini, Removal of Methylene Blue from aqueous solutions by adsorption on kaolin: kinetic and equilibrium studies, Appl. Clay Sci., 153 (2018) 38–45.

[44] K.A. Krishnan, K. Ajmal, A.K. Faisal, T.M. Liji, Kinetic and isotherm modeling of methylene blue adsorption onto kaolinite clay at the solid-liquid interface, Sep. Sci. Technol., 50 (2015) 1147–1157.

[45] K.K. Beltrame, A.L. Cazetta, P.S.C. de Souza, L. Spessato, T.L. Silva, V.C. Almeida, Adsorption of caffeine on mesoporous activated carbon fibers prepared from pineapple plant leaves, Ecotoxicol. Environ. Saf., 147 (2018) 64–71.

[46] M.M. Ayad, A.A. El-Nasr, Adsorption of cationic dye (methylene blue) from water using polyaniline nanotubes base, J. Phys. Chem., 114 (2010) 14377–14383.

[47] P. Sharma, N. Hussain, D.J. Borah, M.R. Das, Kinetics and adsorption behavior of the methyl blue at the graphene oxide/reduced graphene oxide nanosheet–water interface: a comparative study, J. Chem. Eng. Data, 58 (2013) 3477–3488.

[48] A.B. Albadarin, M.N. Collins, M. Naushad, S. Shirazian, G. Walker, C. Mangwandi, Activated lignin–chitosan extruded blends for efficient adsorption of methylene blue, Chem. Eng. J., 307 (2017) 264–272.

[49] F. Bouaziz, M. Koubaa, F. Kallel, R. Ellouz Ghorbel, S. Ellouz Chaabouni, Adsorptive removal of malachite green from aqueous solutions by almond gum: kinetic study and equilibrium isotherms, Int. J. Biol. Macromol., 105 (2017) 56–65.

[50] F. Naseeruteen, N. Shahirah Abdul Hamid, F. Bukhari Mohd Suah, W. Saime Wan Ngah, F. Shimal Mehamod, Adsorption of malachite green from aqueous solution by using novel chitosan ionic liquid beads, Int. J. Biol. Macromol., 107 (2018) 1270–1277.

[51] S. Wang, E. Ariyanto, Competitive adsorption of malachite green and Pb ions on natural zeolite, J. Coll. Interface Sci., 314 (2007) 25–31.

[52] Z. Yin, Y. Wang, K. Wang, C. Zhang, The adsorption behavior of hydroxypropyl guar gum onto quartz sand, J. Mol. Liq., 258 (2018) 10–17.